Liquid Crystals
Publication details, including instructions for authors and subscription information:
http://www.informaworld.com/smpp/title~content=t713926090

Microscopic observations of axial and radial nematic droplets for a dual-frequency addressable liquid crystal

H. -S. Kitzerow[a]; F. Xu[a]; P. P. Crooker[b]
[a] Iwan-N.-Stranski-Institut, Technische Universität Berlin, Berlin 12, Germany [b] Department of Physics and Astronomy, University of Hawaii, Honolulu, Hawaii, U.S.A.

To cite this Article Kitzerow, H. -S. , Xu, F. and Crooker, P. P.(1992) 'Microscopic observations of axial and radial nematic droplets for a dual-frequency addressable liquid crystal', Liquid Crystals, 12: 6, 1019 — 1024
To link to this Article: DOI: 10.1080/02678299208032817
URL: http://dx.doi.org/10.1080/02678299208032817

Liquid Crystals, 1992, Vol. 12, No. 6, 1019–1024

Microscopic observations of axial and radial nematic droplets for a dual-frequency addressable liquid crystal

by H.-S. KITZEROW†, F. XU‡ and P. P. CROOKER‡
† Iwan-N.-Stranski-Institut, Technische Universität Berlin, Sekr. ER 11, Strasse des 17. Juni 135, 1000 Berlin 12, Germany
‡ Department of Physics and Astronomy, University of Hawaii, 2505 Correa Road, Honolulu, Hawaii 96822, U.S.A.

(*Received 8 June 1992; accepted 7 September 1992*)

We report observations on nematic droplets of a dual-frequency addressable nematic mixture using polarization microscopy. When low frequency ($f=100$ Hz) electric fields are applied, the dielectric anisotropy is positive and the droplets show the usual behaviour, i.e. dark polarization rings which move outward with increasing field strength. When high frequency ($f=50$ kHz) fields are applied, however, the dielectric anisotropy is negative and the dark polarization rings move inward with increasing field strength. The appearance of the droplets in transmission is compared to computer-simulated pictures using a simple model which describes the change of the director field within a weak field limit.

1. Introduction

Polymer-dispersed liquid crystals have been extensively studied during the past few years [1, 2] due to their suitability for a variety of applications, for example for flexible displays, switchable windows and projection displays. By using the matching or mismatching of the refractive indices of the liquid crystal droplets and the polymer matrix, polymer-dispersed liquid crystal devices can be switched between an opaque scattering 'off' state and a transparent 'on' state [3]. In most of these applications nematic liquid crystals with positive dielectric anisotropy ε_a are used. However, work on liquid crystals with negative dielectric anisotropy [4] and on dual-frequency addressable materials [5, 6] has also been reported. The latter work was motivated by the development of reverse-mode polymer-dispersed liquid crystal displays [4], which are transparent in the off state and become scattering when a voltage is applied. For display applications, small droplet sizes ($R<1\,\mu$m) are preferred in order to achieve fast switching, but for structural investigations of the droplet director field it is useful to study the textures of large nematic droplets ($R\geqslant 10\,\mu$m) using a polarizing microscope. Such investigations have been reported recently [7] for different nematic structures and their behaviour in electric fields for $\varepsilon_a>0$.

In the present paper we report observations, using polarization microscopy, of large nematic droplets of a dual-frequency addressable liquid crystal which exhibits positive dielectric anisotropy at low frequencies and negative dielectric anisotropy at high frequencies. In addition to the known textural changes for $\varepsilon_a>0$, we also investigated the textural changes for $\varepsilon_a<0$ on the same material. Our preliminary studies are devoted only to systems with homeotropic boundary conditions where a radial and an axial structure are known to occur [7]; a field-induced radial/axial transition has been

* Author for correspondence.

reported [8] for such systems when $\varepsilon_a > 0$. We discuss our observations qualitatively using a simple model which is valid for small field strengths, i.e. below the threshold for the radial/axial transition.

2. Experimental

The liquid crystal under investigation is the mixture ZLI 2461 (E. Merck, Germany) which exhibits a wide nematic temperature range. When a sinusoidal electric field of frequency $f_r = 2{\cdot}3$ kHz is applied, the dielectric anisotropy is zero. As the frequency is decreased below f_r, ε_a becomes increasingly positive, while above f_r, ε_a becomes increasingly negative. Instead of using a polymer matrix we dispersed the liquid crystal in glycerol. Homeotropic alignment at the droplet surfaces was achieved by doping the glycerol with approximately 0·1 per cent lecithin. Gentle stirring of the dispersion led to different droplet sizes with radii from $R < 1\ \mu$m to $R \approx 50\ \mu$m. The dispersion was placed between two ITO coated glass slides separated by $50\ \mu$m spacers. Voltages up to 180 V (rms) were applied at frequencies of 100 Hz ($\varepsilon_a = +2{\cdot}4$) and 50 kHz ($\varepsilon_a = -1{\cdot}9$), respectively [9].

At zero voltage, the texture between crossed polarizers indicates an axial director configuration [7] for many droplets (see figure 1 (*a*)). When viewed along the *z* axis, this texture is characterized by concentric dark rings and a broad Maltese cross (see figure 2 (*b*)). Some larger droplets ($R \geqslant 10\ \mu$m) exhibit a radial structure (see figure 1 (*b*)), which can be identified in the polarizing microscope by a very sharp dark cross in the droplet centre (see figure 2 (*e*)) [7]. The dependence of the director configuration on the droplet size is in agreement with earlier observations [8], but coexistence of both radial and axial droplets occurs for a broad range of droplet sizes in our sample. In addition to radial and axial droplets we also found droplets showing a spiral in their centre, as observed earlier [10, 11]. In this paper, however, we concentrate on the droplets with radial and axial configurations. The much more complicated behaviour of the spiral droplets will be discussed in a forthcoming paper [12].

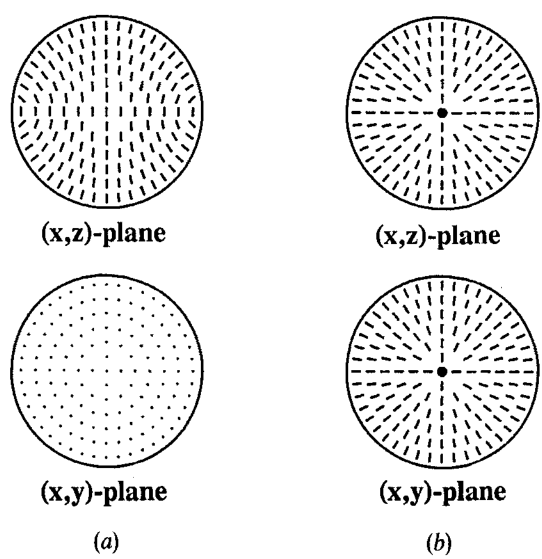

Figure 1. Director field of (*a*) an axial and (*b*) a radial droplet.

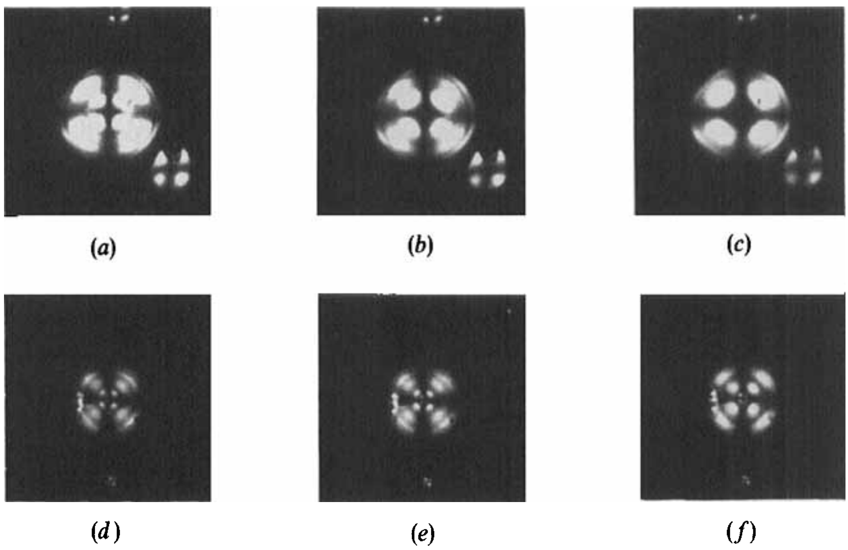

Figure 2. Microphotographs of an axial (*a*)–(*c*) and a radial droplet (*d*)–(*e*) for different electric fields. (*a*) Axial, $\varepsilon_a < 0$, $E = 3{\cdot}2\,V\,\mu m^{-1}$, $f = 50\,kHz$; (*b*) axial, $E = 0$; (*c*) axial, $\varepsilon_a > 0$, $E = 3{\cdot}2\,V\,\mu m^{-1}$, $f = 100\,Hz$; (*d*) radial, $\varepsilon_a < 0$, $E = 1{\cdot}8\,V\,\mu m^{-1}$, $f = 50\,kHz$; (*e*) radial, $E = 0$; (*f*) radial, $\varepsilon_a > 0$, $E = 3{\cdot}6\,V\,\mu m^{-1}$, $f = 100\,Hz$.

Under the influence of weak electric fields, the Maltese cross for both radial and axial droplets is preserved, which indicates that the projection of the director in the plane perpendicular to the field remains radial. However the diameter of the concentric rings changes continuously with field strength, thereby indicating a change of the effective birefringence for light propagating along the field direction. For increasing field, the diameters decrease for $\varepsilon_a < 0$ (see figure 2 (*a*) and (*d*)) and increase for $\varepsilon_a > 0$ (see figures 2 (*c*) and (*f*)).

The increase in ring diameter for $\varepsilon_a > 0$ is similar to the textural change corresponding to the field-induced radial/axial transition [8]. This transition was not observed in our drops, however, since only voltages less than those required for the transition were applied. In addition, since the radial configuration exhibits a hedgehog defect and the axial configuration shows an equatorial disclination ring, we might expect the hedgehog defect to evolve into a disclination ring as the field is increased, starting from radius $r = 0$ (radial) to $r = R$ (axial) [13]. To check this possibility, we examined the central defect in radial drops; this defect can be seen in the microscope without polarizers. No change of the central defect to a ring was observed up to $E = 3{\cdot}6\,V\,\mu m^{-1}$. We conclude that the topology of the radial director field is preserved when the applied field is not large.

3. Discussion

In order to explain the experimental results, we have calculated the polarized transmission patterns from model director configurations in order to compare them to the observed experimental patterns. Consider a light beam which propagates through the droplet along the z direction of a cartesian coordinate system, and let the droplet be divided into layers of equal thickness $h = R/100$ which are parallel to the (x, y) plane.

Each of these layers behaves like a uniaxial optical retarder, i.e. at any point (x, y) it introduces a phase shift

$$\delta_i(x,y) = 2\pi[n_{e,\mathrm{eff}}(x,y) - n_o]h/\lambda \quad (1)$$

between the linearly polarized light components parallel and perpendicular to the azimuthal orientation of the director, Here n_o is the ordinary refractive index, n_e is the extraordinary refractive index, and $n_{e,\mathrm{eff}}$ is the effective extraordinary refractive index at point (x, y) of the layer, which depends on the angle between the director $\mathbf{n}$ and the direction of light propagation according to

$$n_{e,\mathrm{eff}} = [\sin^2\beta/n_e^2 + \cos^2\beta/n_o^2]^{-1/2}. \quad (2)$$

In general, both the orientation of the optic axis and the retardation may vary from layer to layer. However, for the special case of radial and axial director fields $\mathbf{n}(\mathbf{r})$, the azimuthal orientation φ of the director at given (x, y) is the same for all layers. Thus it is not necessary to calculate the change of the light ellipticity for each individual layer, but we can simply calculate the transmitted intensity from the total phase shift δ using the relation

$$I(\varphi,\delta) = \tfrac{1}{2}I_0 \sin^2 2\varphi \sin^2 \tfrac{1}{2}\delta. \quad (3)$$

The total phase shift $\delta(x, y)$ is the sum of the phase shifts $\delta_i(x, y)$ caused by the different layers. Due to the rotational symmetry of radial and axial droplets, δ depends only on the distance $\rho = (x^2 + y^2)^{1/2}$ of the transmitted beam from the central axis of the droplet. Figure 3 shows δ versus ρ/R for ε_a positive, negative, and zero; note that the curve labeled $\varepsilon_a = 0$ also represents the phase shifts for any ε_a when $E = 0$. The radius of the concentric dark rings in the droplet texture corresponds to values ρ where the retardation δ is equal to 2π times an integer. Thus if we take the case of $\varepsilon_a < 0$ and increase E gradually from zero, the phase shifts progress from the $\varepsilon_a = 0$ curve to the $\varepsilon_a < 0$ curve in figure 3. As E increases, the inner circles move toward the centre, the outer circles toward the droplet periphery, and new rings may appear between them. For the case of $\varepsilon_a > 0$ and increasing field, the opposite happens: here the inner rings move radially outward, the other rings move radially inward, and rings between may even vanish.

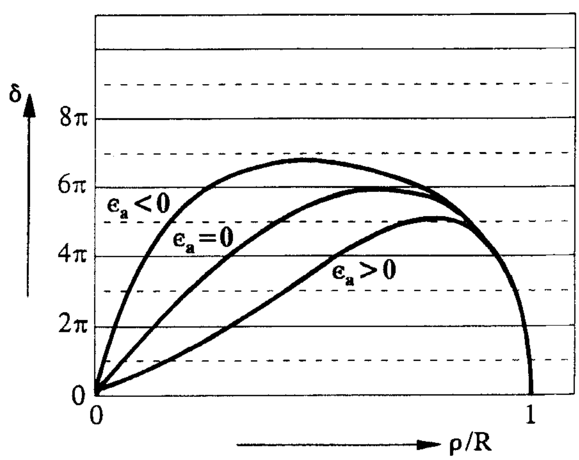

Figure 3. (*a*) Retardation δ versus cylindrical coordinate ρ/R for a nematic droplet ($R = 16\,\mu$m, $\Delta n = 0{\cdot}1$) for $\varepsilon_a < 0$, $\varepsilon_a = 0$, and $\varepsilon_a > 0$ (the corresponding parameters are given in figure 4).

In order to describe mathematically the influence of electric fields on the director configuration, we denote the position within a droplet by the usual polar coordinates (r, θ, φ) and the director orientation by a polar angle β and an azimuthal angle γ. In the case where $E=0$, we set $\beta=\beta_0$ and $\gamma=\gamma_0$. Thus for a purely radial droplet, the director angles are given by $\beta_0=\theta$ and $\gamma_0=\varphi$. For an axial droplet, the projection of the director in the (x, y) plane is also radial $(\gamma_0=\varphi)$, but the angle β_0 between the z axis and the director is given by

$$\beta_0=\theta+\arctan[(1+r^2/R^2)(1-r^2/R^2)^{-1}(\tan\theta)^{-1}]+\pi/2. \quad (4)$$

For $r=R$ or $\theta=0$ where equation (4) is not defined, the director orientation is radial. We assume that the application of an electric field along the z direction causes only β to change, that is, $\beta_0 \rightarrow \beta$. This angle is shifted either towards $\beta_1=\pi/2$ (for $\varepsilon_a<0$) or towards $\beta_1=0$ or π (for $\varepsilon_a>0$). There are many mathematical forms for such a shift; in our case, we arbitrarily use the expression

$$\beta=\beta_0+(\beta_1-\beta_0)|\sin 2\theta|\{1-\exp[-(R-r)/\xi]\}. \quad (5)$$

For $\varepsilon_a>0$, $\beta_1=\pi/2$; for $\varepsilon_a<0$, $\beta_1=0$ when $\beta_0<\pi/2$ and $\beta_1=\pi$ when $\beta_0>\pi/2$. The term $|\sin 2\theta|$ prevents director rotation at $\theta=0, \pi/2$, and thus preserves mirror symmetry of the droplet about the equator. Finally, the exponential term in brackets ensures that the

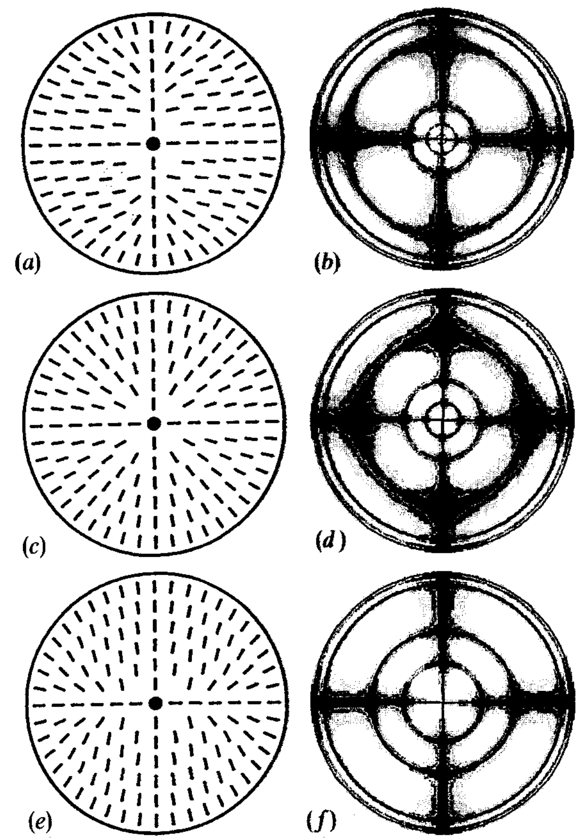

Figure 4. Director configurations and corresponding transmission patterns calculated from equation (5); (*a*), (*c*), (*e*) are director configurations; (*b*), (*d*), (*f*) are the corresponding transmission patterns using the data of figure 3. The parameters are: (*a*), (*b*) $\beta_1=\pi/2$, $\xi=0{\cdot}7\,R$; (*c*), (*d*) $\beta_1=\beta_0$; (*e*), (*f*) $\beta_1=0$ for $\theta\leqslant\pi/2$, $\beta_1=\pi$ for $\theta>\pi/2$, $\xi=0{\cdot}7\,R$.

homeotropic boundary condition is preserved to a radial depth ξ in the droplet. We emphasize, however, that equation (5) is only a reasonable approximation of the true director field; a calculation of the exact director field, which is a result of a minimization of the elastic energy, surface anchoring energy, and electric field alignment energy, is beyond the scope of this paper.

Figure 4 shows how the director configuration affects the transmission pattern for radial droplets. Figure 4 (*a*) shows the director field in the (x, z) plane calculated from equation (5) for $\varepsilon_a < 0$. The increase of the director polar angle β has no effect on n_o, but $n_{e,\,eff}$ is clearly increased as required by equation (2). Figure 4 (*b*) shows the calculated transmission pattern using the same director configuration, and is meant to approximate figure 2 (*d*). Figures 4 (*c*) and (*d*) show the director field and calculated transmission pattern for $\varepsilon_a = 0$ (or equivalently, $E = 0$), while figures 4 (*e*) and (*f*) show the results for $\varepsilon_a > 0$. Figures 4 (*b*), (*d*) and (*f*) should be compared with figure 3 and with the experimental data of figures 2 (*d*)–(*f*). The droplet photographs do not reveal the fine details of the calculated patterns, but qualitatively it can be seen that figures 2 and 4 are in agreement.

4. Conclusions

In conclusion, we have investigated the behaviour of dual-frequency addressable nematic droplets in electric fields by means of polarization microscopy. The patterns observed in transmission consist of a dark cross and dark concentric rings which change their diameters with changing electric field in a direction dependent on the sign of the dielectric anisotropy. These changes can be described by a variation of the director field which does not affect the topology of the disclinations within the droplet structure. However, for high fields, topological changes of the director field must also be considered, such as the radial/axial transition reported for positive dielectric anisotropy [8]. These more complex transformations and the behaviour of droplets showing a spiral pattern are the subject of further investigations.

We would like to thank R. Jubb and U. Finkenzeller (E. Merck, Germany) for supplying us with ZLI 2461. This work was supported by the Deutsche Forschungsgemeinschaft (Sfb 335) and by the Cottrell Foundation-Research Corporation.

References

[1] Doane, J. W., Golemme, A., West, J. L., Whitehead, J. B., and Wu, B.-G., 1988, *Molec. Crystals liq. Crystals*, **165**, 511.
[2] Doane, J. W., 1990, *Liquid Crystals—Applications and Uses*, vol. 1, edited by B. Bahadur (World Science Publishers), p. 361.
[3] Doane, J. W., Vaz, N. A., Wu, B.-G., and Žumer, S., 1986, *Appl. Phys. Lett.*, **48**, 269.
[4] Ma, Y.-D., Wu, B.-G., and Xu, G., 1990, *S.P.I.E.*, **1257**, 46.
[5] Lackner, A. M., Margerum, D., Ramos, E., Smith, W. H., and Kim, L. C., 1990, United States Patent No. 4 944 576.
[6] Nolan, P., and Coates, D., 1991, *Molec. Crystals liq. Crystals Lett.*, **8**, 75.
[7] Ondris-Crawford, R., Boyko, E. P., Wagner, B. G., Erdmann, J. H., Žumer, S., and Doane, J. W., 1991, *J. appl. Phys.*, **69**, 6380.
[8] Erdmann, J. H., Žumer, S., and Doane, J. W., 1990, *Phys. Rev. Lett.*, **64**, 1907.
[9] Material parameters according to the producing company E. Merck (Darmstadt, Germany).
[10] de Gennes, P. G., 1974, *The Physics of Liquid Crystals* (Clarendon Press).
[11] Lavrentovich, O. D., and Terent'ev, E. M., 1986, *Sov. Phys. J.E.T.P.*, **64**, 1237.
[12] Xu, F., Kitzerow, H.-S., and Crooker, P. P., 1992, *Phys. Rev.* A (in the press).
[13] Kilian, A., 1991 (private communication).